

## Invited Article: CO<sub>2</sub> laser production of fused silica fibers for use in interferometric gravitational wave detector mirror suspensions

A. Heptonstall,<sup>1,2,a)</sup> M. A. Barton,<sup>1</sup> A. Bell,<sup>2</sup> G. Cagnoli,<sup>3</sup> C. A. Cantley,<sup>2</sup> D. R. M. Crooks,<sup>2</sup> A. Cumming,<sup>2</sup> A. Grant,<sup>2</sup> G. D. Hammond,<sup>2</sup> G. M. Harry,<sup>4</sup> J. Hough,<sup>2</sup> R. Jones,<sup>2</sup> D. Kelley,<sup>4</sup> R. Kumar,<sup>2</sup> I. W. Martin,<sup>2</sup> N. A. Robertson,<sup>1,2</sup> S. Rowan,<sup>2</sup> K. A. Strain,<sup>2</sup> K. Tokmakov,<sup>2</sup> and M. van Veggel<sup>2</sup>

<sup>1</sup>LIGO Laboratory, California Institute of Technology, Pasadena, California 91125, USA

<sup>2</sup>SUPA, Institute for Gravitational Research, University of Glasgow, Glasgow G12 8QQ, United Kingdom

<sup>3</sup>Istituto Nazionale di Fisica Nucleare, Sezione di Firenze, Sesto Fiorentino I-50019, Italy

<sup>4</sup>LIGO Laboratory, Massachusetts Institute of Technology, Cambridge, Massachusetts 02139, USA

(Received 13 September 2010; accepted 6 November 2010; published online 21 January 2011)

In 2000 the first mirror suspensions to use a quasi-monolithic final stage were installed at the GEO600 detector site outside Hannover, pioneering the use of fused silica suspension fibers in long baseline interferometric detectors to reduce suspension thermal noise. Since that time, development of the production methods of fused silica fibers has continued. We present here a review of a novel CO<sub>2</sub> laser-based fiber pulling machine developed for the production of fused silica suspensions for the next generation of interferometric gravitational wave detectors and for use in experiments requiring low thermal noise suspensions. We discuss tolerances, strengths, and thermal noise performance requirements for the next generation of gravitational wave detectors. Measurements made on fibers produced using this machine show a 0.8% variation in vertical stiffness and 0.05% tolerance on length, with average strengths exceeding 4 GPa, and mechanical dissipation which meets the requirements for Advanced LIGO thermal noise performance. © 2011 American Institute of Physics. [doi:10.1063/1.3532770]

### I. INTRODUCTION

One of the limiting sources of noise in interferometric gravitational wave detectors is the thermally driven motion of the mirrors and their suspensions. According to the fluctuation-dissipation theorem,<sup>1–5</sup> thermal noise may be reduced at detection band frequencies by use of ultralow dissipation materials. The power spectral density of thermally induced displacement noise for a pendulum, at frequencies well above resonance, may be written as

$$S_x(\omega) = \frac{4k_B T \omega_0^2}{m \omega^5} \phi(\omega), \quad (1)$$

where  $\omega$  is the angular frequency,  $m$  is the suspended mass,  $T$  is the temperature,  $\omega_0$  is the pendulum angular resonant frequency,  $k_B$  is the Boltzmann constant, and  $\phi(\omega)$  is the pendulum loss angle. Fused silica is one such low dissipation material suitable for interferometric gravitational wave detectors.<sup>6–11</sup> Dissipation in fused silica is several orders of magnitude lower than in metals.<sup>12–14</sup>

Friction in the joints of the mirror suspensions also contributes to detection band thermal noise.<sup>15</sup> GEO600 is the first detector to use a quasi-monolithic final stage in the mirror suspensions to reduce this friction.<sup>16</sup> Figure 1(a) shows one of the GEO600 triple suspensions. Attachment blocks are hydroxide-catalysis bonded to the GEO600 optics.<sup>16–19</sup> The optic is then suspended using four flame-pulled fused silica fibers that are gas-welded to the attachment blocks.<sup>20</sup>

Following the success in GEO600, where a total of 20 fibers have suspended the optics for over eight years with no evidence of unexpected problems,<sup>21</sup> planned upgrades to the LIGO and Virgo detectors will include installation of quasi-monolithic final stage suspensions.<sup>22,23</sup> Figure 1(b) shows a SOLIDWORKS® (Ref. 24) rendering of an Advanced LIGO quadruple mirror suspension.

Thermoelastic damping<sup>25–27</sup> ( $\phi_t$ ), frequency dependent bulk dissipation<sup>11,28</sup> ( $\phi_b$ ), and dissipation in the surface layer<sup>29</sup> ( $\phi_s$ ) all contribute to the total loss angle of the pendulum. The loss of the pendulum mode is reduced by the dilution factor ( $D$ ), given by the ratio of energy stored in lifting the mass against gravity to energy stored in flexing the fiber. The total loss of the pendulum mode may be written as

$$\phi(\omega) = D(\phi_t + \phi_b + \phi_s). \quad (2)$$

For thin fibers bulk loss is negligible compared to dissipation from the lossy surface layer.<sup>11,30,31</sup> Each of the other components is dependent on the diameter of the flexure point, with dilution also being dependent on fiber length.

The average fiber diameter sets the frequency for certain other modes of oscillation of the suspension. The mode in which the test mass moves vertically up and down is known as the vertical bounce mode and the frequency of this affects coupling of vertical noise into the detector.<sup>32,33</sup> The strength of the fiber ultimately limits how low the vertical bounce frequency can be made. The modes in which the masses above and below the fibers stay approximately stationary while the fibers oscillate are known collectively as the violin modes since the fibers move in a similar manner to the strings of a

<sup>a)</sup>Electronic mail: heptonstall\_a@ligo.caltech.edu.

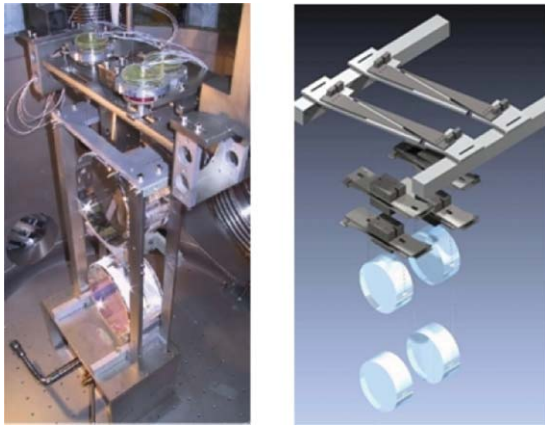


FIG. 1. (Color) Gravitational wave detector mirror suspensions. (a) GEO600 triple suspension. (b) SOLIDWORKS rendering of an Advanced LIGO quadruple suspension.

stringed instrument. The fiber diameter also sets the frequency of fiber violin modes. For all current interferometric detectors, the lowest frequency violin modes occur in the detection band of the interferometer, where the small motions of the test mass they cause must be notched out of the data. It is preferable to have the violin mode frequencies as high as possible by keeping the fiber diameter small.

For a mass suspended close to the center of mass, the dilution effect is given by<sup>34</sup>

$$D = \frac{1}{L} \sqrt{\frac{Y\pi r^4}{4T}}, \quad (3)$$

where  $Y$  is the Young's modulus of the fibers,  $r$  is the radius of the fibers,  $L$  is the fiber length, and  $T$  is the tension in each fiber. The dissipation in the surface layer may be modeled as<sup>29</sup>

$$\phi_s = 8 \frac{h}{2r} \phi_{\text{surface}}, \quad (4)$$

where  $h$  is the thickness of the lossy surface layer and  $\phi_{\text{surface}}$  is the loss angle of this layer. The thermoelastic loss for a fiber under tension is given by the nonlinear thermoelastic theory<sup>27</sup>

$$\phi_t = \left( \frac{YT}{\rho C} \right) \left( \frac{\omega\tau}{1 + (\omega\tau)^2} \right) \left( \alpha - \beta \frac{mg}{Y\pi r^2} \right)^2, \quad (5)$$

where  $\rho$  is the density,  $\alpha$  is the thermal expansion coefficient,  $C$  is the specific heat capacity, and  $\beta$  is the fractional change in Young's modulus with temperature. The characteristic time for heat transfer across a cylindrical fiber,  $\tau$ , is given by

$$\tau = \frac{\rho C d^2}{4.32\pi\kappa}, \quad (6)$$

where  $\kappa$  is the thermal conductivity.

From Eq. (5), we see that for a given mass, it is possible to cancel the thermoelastic contribution completely by using a particular fiber diameter. For a 40 kg mass suspended on four fibers, this corresponds to approximately  $r = 410 \mu\text{m}$  depending on the exact values of the material properties. From Eq. (3), it can be seen that the dilution effect increases as the fiber diameter decreases and it is of interest to note that while the thermoelastic loss may be canceled for a given diameter

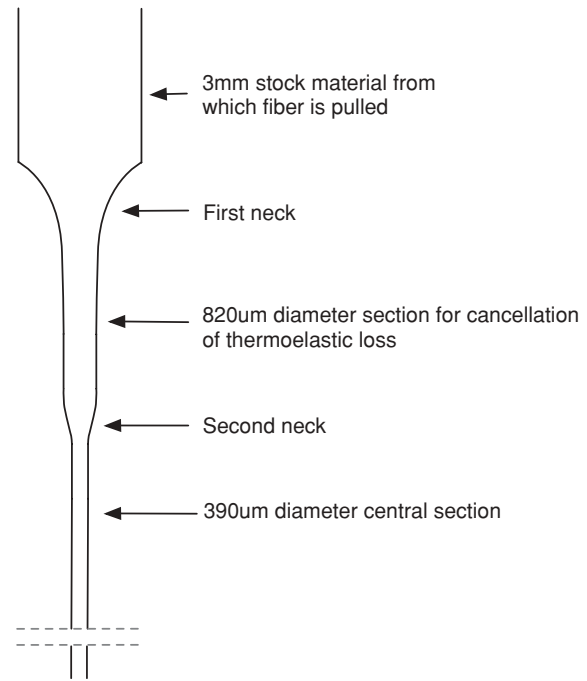


FIG. 2. Diagram showing the profile of one end of a dumbbell shaped fiber.

of fiber, the dilution effect is reduced since the ends of the fiber are thicker. However, there is a minima in the total loss for this diameter, giving a lower thermal noise.

The baseline design for Advanced LIGO is a dumbbell design of fiber,<sup>35,36</sup> where the diameter of the flexure points is set to cancel thermoelastic noise, while the middle of the fiber is thinned down to reduce the bounce frequency ( $<10$  Hz) and increase the first violin mode resonance ( $>500$  Hz). Figure 2 shows a schematic of the varying diameter profile of a dumbbell shaped fiber. The fiber pulling system must be capable of creating this varying diameter shape.

Fiber diameter, length, and placement also affect the pitch, yaw, and roll of the mirror, altering the coupling of noise into the horizontal direction. Modeling of the Advanced LIGO quadruple suspension<sup>32,33,37</sup> sets a required tolerance of 2.8% for the vertical stiffness of the fiber, and a positioning of the flexure point of approximately 0.1 mm parallel to the optical axis and 1 mm vertically. In addition to this the violin mode frequencies, which must be notched out of control systems, should be kept as close together as possible, approximately within 1 Hz of each other. For the first violin mode this gives a fiber length tolerance of 1.2 mm, and for the second violin mode, a length tolerance of 0.6 mm.

The static stress on the fibers will be 0.8 GPa and it is a technical requirement that the failure point of the fibers be at least three times this value. The suspension is constrained in a structure that prevents the fibers stretching by more than the equivalent of an additional 20% loading.

Silica fibers have been produced by a variety of methods,<sup>30,31,38-40</sup> though all follow a common theme. The thin fibers are drawn from a thicker stock material that is heated until molten and then pulled. Techniques for producing fused silica fibers by hand in a hydrogen-oxygen flame have existed for some time.<sup>38</sup> While it is possible to produce individual fibers by hand, some degree of automation is

required to meet the consistency requirements of gravitational wave detector mirror suspensions.

The fibers used in the GEO600 mirror suspensions were produced using an automated pulling machine, using a hydrogen–oxygen flame to heat the silica until molten. The machine used a “heat then pull” method whereby the total amount of silica required for the fiber was heated, then the flame was removed and the fiber was pulled by two chain-driven arms mounted on linear bearings.

To test and characterize the fibers they were loaded and bounce tested to measure their vertical stiffness. They were then grouped according to length and bounce frequency before being used to suspend the optics. A tolerance of 3.1% was achieved for the bounce frequency of the individual fibers, corresponding to an error of 2.1% in length and cross section of the fibers.<sup>33</sup> The reproducibility of fibers from this machine is limited by both backlash in the mechanics and variations in gas flow to the burners.

We present in this paper a description of a novel CO<sub>2</sub> laser-based fiber pulling machine developed at the University of Glasgow. This laser-based system has been developed with a view to creating high precision, high strength, and ultralow loss fused silica fibers for the second generation gravitational wave detectors such as the planned upgrades to LIGO and Virgo. At present three such machines have been built, with a prototype at the University of Glasgow and further machines installed at the Virgo detector site and LIGO’s LASTI test facility at the MIT.

Fibers produced using this system have also been used in experiments to measure force noise arising from the capacitive sensors and residual gas for the LISA and LISA Pathfinder missions.<sup>41,42</sup>

CO<sub>2</sub> lasers have previously been used to create thin fused silica fibers of 1–20  $\mu\text{m}$  diameter,<sup>43</sup> elliptical fused quartz lightguides,<sup>44</sup> and to weld 65  $\mu\text{m}$  diameter fused silica fibers.<sup>45</sup> The thin fused silica fibers described in Ref. 43 were produced using a method in which the fiber is heated continuously while under constant tension from a suspended mass, until such a diameter is achieved that the power radiated from the surface is equal to the laser power absorbed. Using this method the fiber tolerances depend only on the stability of the laser and not on mechanics. However, this can only be achieved for very thin fibers, where the diameter is approximately the same as the wavelength of the incident laser light, and as such is not a suitable method for producing fibers of several hundred microns diameter. The lightguides described in Ref. 44 were made using a deliberately asymmetric laser heating arrangement to produce an elliptical cross-section core. This anisotropy is required to preserve the state of polarization of the electromagnetic field as it propagates through the lightguide. With the system we describe here, we wish to achieve the opposite of this, to produce highly symmetric fibers. The fiber welding described in Ref. 45 was used to weld thin fibers without necks by heating from one side. To obtain a high strength joint the fibers used in gravitational wave detector mirror suspensions are typically welded at the neck that has a diameter of 3 mm and must be heated from multiple directions.

The new machine was designed to significantly improve both drive mechanics and heat delivery. There are several advantages to using a laser as the heat source. Heating with a laser produces a minimum of by-products. In particular there is no water produced as there is no hydrogen–oxygen. Water is known to attack the surface of fused silica, causing the propagation of surface cracks<sup>46</sup> that reduce strength and reduce thermal noise performance by increasing dissipation. The blowing of a flame across the surface of the fused silica can also cause particulate matter from the air or burners to contaminate the fiber surface. In addition, power stabilization allows lasers to provide a highly stable and predictable source of heat.

## II. DESIGN OF THE CO<sub>2</sub> LASER PULLING MACHINE

Two versions of the fiber pulling system were developed. One design was built to produce tapered cylindrical cross-section fibers, while a second design was developed for rectangular cross-section fibers known as ribbons. Both types of fiber could be used to meet the performance requirements for the Virgo and LIGO upgrades, and offer different advantages.

In a suspension system ribbons are more compliant in the direction of measurement than a similar cross-sectional area cylindrical fiber allowing them to appear thinner. This gives a higher dilution effect which in turn reduces thermal noise. In practice the shape of the flexure region of the ribbon is critical and can cause a significant reduction in dilution if the flexure point is thicker than intended. This typically happens because of the “neck” region of the fiber, the part at either end where it increases in diameter up to the stock material from which it is pulled.<sup>47,48</sup> The neck is usually retained to allow easy welding of the fiber.

A tapered cylindrical fiber allows the thermoelastic component of the dissipation to be canceled out by balancing the thermal expansion of the fiber against the thermal-expansion-like effect of the static stress in a material with a positive temperature dependent stiffness. Both ribbon and tapered cylindrical fiber designs are reasonable solutions to meeting the required noise performance for Advanced LIGO; however, for reasons of ease of manufacture and reproducibility, tapered cylindrical fibers have now replaced ribbons as the baseline for the Advanced LIGO detector.<sup>36</sup>

A tapered ribbon still offers a slight advantage over the tapered cylindrical fiber by giving an extra degree of freedom in designing the fibers, since the thickness in the direction of measurement is not fixed by the cross-sectional area as it is for a cylindrical fiber. For the Advanced LIGO detector suspensions, the advantage gained from a practical implementation of this is only at the level of a few percent, but it may be possible to gain a further advantage in future detector suspension designs. The ribbon pulling machine described here is the first to produce tapered fused silica ribbons.

The two designs of machine share the same underlying drive mechanics and laser heat source, but have different beam delivery systems and computer control systems. We shall first discuss the shared parts before looking at the differences in the two designs.

The drive system used for both designs is based on precision recirculating ball screws. This type of rotation to translation converter has the lowest backlash compared to other types such as leadscrews, belt, or chain drives. They are typically chosen for applications involving high loads and where high precision is required over the lifetime of the device. Two 1 m long ball screw units are mounted vertically, providing the drive for the upper and lower carriages. The positional repeatability in these units is quoted by the manufacturer to be 50  $\mu\text{m}$ .

The vertical bearing units are powered by two digital servo-driven electric motors capable of generating 4.2 Nm of torque. The motors contain high resolution encoders, giving  $2 \times 10^6$  counts per rotation that are used for velocity feedback in the motor controller. The output of each motor drives a 1:5 reduction gearbox, increasing the maximum torque to 21 N m. The maximum force applied by the system on the carriages is limited by the structural strength of the ball screw to 1000 N, with the motors capable of applying approximately ten times this force. The force required to pull a fiber is a small fraction of this limit. Such an overspecified system was designed primarily to ensure that any small variation in the force required during the pull would not translate into a variation in the speed of the pull. The maximum speed and acceleration are also limited by the ball screw unit which is rated for 250 mm/s and 5  $\text{m/s}^2$ , respectively. The motor speeds are controlled by a custom LABVIEW program.

The position of the upper and lower carriages is measured using magnetic linear encoders with 0.1 mm resolution. The position of the carriages is fed back to the control program to control the fiber profile. For each encoder count the program reads in a new speed value for the motors from a data file. In this way a number of fiber designs can be stored and produced at will. In practice the position of the carriages when driven with a typical fiber data file is reproducible to approximately three encoder counts, or 0.3 mm for the faster motor and one encoder count, or 0.1 mm for the slower motor. The faster carriage is thought to be limited by the inertia of the carriage coupled with some mechanical backlash in the system, while the slower carriage is limited by the encoder. The main source of the backlash is in the motor couplings to the ball screws as well as in the ball screw unit itself. The parts mounted horizontally from the ball screw carriage will increase the backlash significantly over manufacturer figures, which are for an unloaded carriage.

The  $\text{CO}_2$  laser can be power stabilized using a proportional-integral-derivative (PID) control system. A small fraction of the laser beam is picked off using a ZnSe Brewster window mounted near the Brewster angle, as shown in Fig. 3. The power of this pick-off beam is measured using a mercury-cadmium-telluride photodiode, with the signal being fed back to the computer. A PID system running on the control computer is used to generate an error signal that is fed back to the laser. In operation when using the power stabilization system, the laser is typically allowed to stabilize for some time by using a mechanical shutter before the fiber pulling routine is started. Using this system the laser power can be stabilized to better than 1% over timescales of tens of minutes. In practice the laser is stable enough after warming

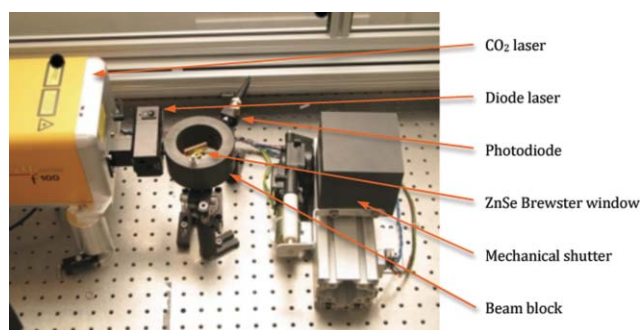


FIG. 3. (Color) Power stabilization system. A small percentage of the laser power is picked off using a ZnSe Brewster window and measured using a photodiode. A graphite beam block is used to remove unwanted reflections.

up to be run without using the power stabilization when producing fibers where the dimensional tolerances are not critical and when performing welds.

### A. Producing cylindrical cross-section fibers

Figure 4 shows the design of the cylindrical fiber pulling machine in SOLIDWORKS. Fibers are pulled from fused silica rod by heating and using a feed-pull method to produce the fiber. The rod must be heated in a uniform way in order to produce a cylindrical cross-section fiber. Figure 5 shows the optical layout that allows a section of the rod to be heated from all sides giving a perfectly symmetric uniform heating about the central vertical axis of the stock. The beam is fed onto an upper fixed mirror, angled at  $45^\circ$  to vertical, which reflects it down onto another  $45^\circ$  mirror that is spinning at approximately 20 rps. This spinning mirror scans the beam around the inside surface of a conical mirror, from where it is reflected upward, forming a cylinder of light. This cylinder hits another conical mirror that reflects the beam inward and onto the stock material. In this way, the stock is heated from all sides, and a uniform heat delivery is achieved. With the current 130 W  $\text{CO}_2$  laser, rods with diameters of up to 5 mm can be used.

The lower part of the cylindrical fused silica rod is fixed in a clamp that is fixed to the base of the machine. The upper end of the rod is fixed in a clamp that it attached to the upper movable arm. As the fiber is heated, the stock material is fed into beam path by moving the lower arm holding the upper conical mirror down over the stock. At the same time the fiber is drawn out of the melt by moving the upper arm upward. The volume of silica fed into the melt matches that pulled from the melt, and thus the diameter of fiber produced can be calculated simply from the starting rod diameter and the speeds of the two carriages. Figure 6 shows a photograph of a cylindrical fiber being pulled from a 3 mm silica rod.

### B. Producing rectangular cross-section fibers

A number of design changes were made to the pulling machine to produce ribbons. These are pulled from a rectangular piece of fused silica stock with the same aspect ratio as the desired final fiber. For Advanced LIGO the original baseline design was to use 60 cm long by 1 mm  $\times$  0.1 mm ribbons,



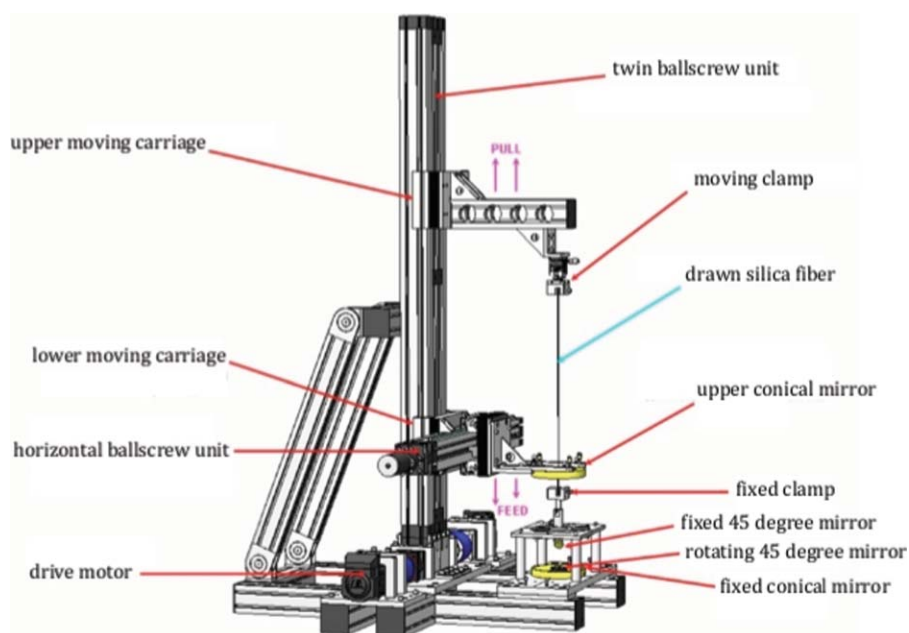


FIG. 4. (Color) SOLIDWORKS rendering of the fiber pulling machine in cylindrical fiber configuration. The functions of all parts are described in the text.

which were pulled from 10:1 aspect ratio fused silica slides 110 mm long by 5 mm  $\times$  0.5 mm. Having chosen the correct aspect ratio, the dimensions of the stock material were picked to give a suitable shaped end to weld onto an ear on the side of a test mass.

To heat the rectangular stock, the conical mirror beam delivery system is replaced by a single mirror galvanometer mounted on a rigid post in front of the machine. This machine setup is shown in Fig. 7. The galvanometer is driven with a signal to dither the beam across the piece of stock to achieve an even heating. Due to the extra heat loss at the edges of the stock, it is necessary for the beam to spend more time over these regions. A cylindrical polished steel heat shield, as shown in Fig. 8, was designed to sit around the stock material during heating to reflect heat back at the edges, reducing

the heat loss. The galvanometer is driven using an arbitrary waveform generator with a trapezoidal waveform. The sloping edge of the trapezoid moves the heat uniformly across the slide surface, while the flat top and bottom of the trapezoid can be lengthened or shortened to alter the relative heating of the edges of the slide. The galvanometer is servo controlled and uses a low mass mirror allowing it to be used up to several kilohertz. While the actual rate of the galvanometer is much lower than this, it is necessary to have good high frequency response to generate both square wave and triangle shapes which have higher order mode content.

The fused silica stock is fixed into clamps that are attached to the upper and lower carriages. With the height of the laser beam now fixed relative to the optical table, the silica stock is fed into the beam by moving the lower carriage upward. The fiber is simultaneously pulled by moving the upper carriage at a higher speed than the lower carriage. Again it

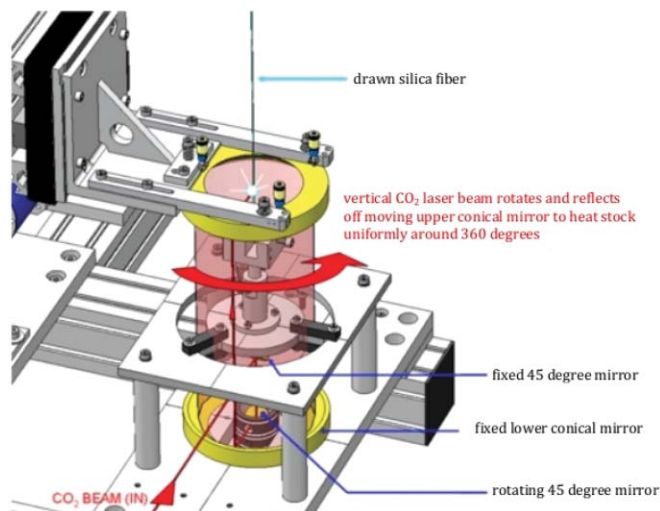


FIG. 5. (Color) Rendered drawing of the laser beam delivery for cylindrical fiber production.



FIG. 6. (Color) The 3 mm diameter cylindrical fused silica stock being heated by the CO<sub>2</sub> laser as the fiber is pulled.

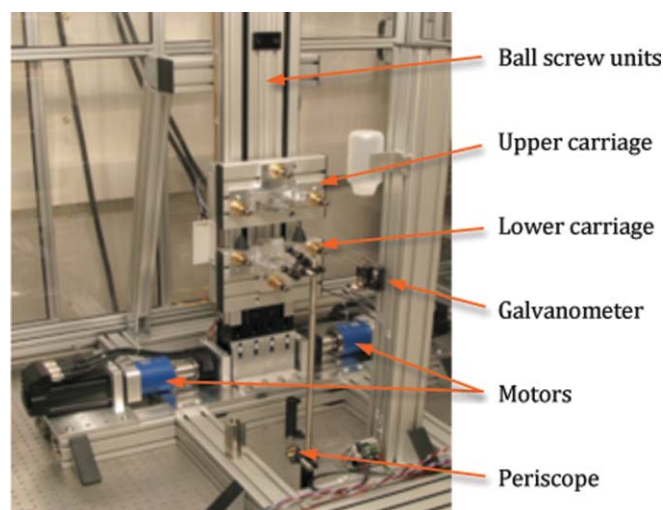


FIG. 7. (Color) Rectangular cross-section fiber pulling machine. Ribbons are pulled from rectangular silica slides. The laser is dithered across the surface using a mirror galvanometer seen here at the front right hand side.

is simple to calculate the ratio of reduction in cross-sectional area based on the speed of the two carriages.

The heating control was found to be more critical when pulling ribbons than for cylindrical fibers. When the silica begins to melt and becomes less viscous, the surface tension acts to pull the fiber toward a cylindrical geometry. If the silica is heated hot enough it is in fact possible to pull a cylindrical cross-section fiber from the rectangular stock. By controlling the laser power it is possible to control the shape of the cross section such that a ribbon with 10:1 aspect ratio is produced.

In practice this relationship between heating and cross-sectional shape puts a constraint on the way in which ribbon fibers can be manufactured that is not seen with cylindrical fibers, limiting the temperature to which the silica can



FIG. 8. (Color) Photograph of a ribbon being pulled. The heating zone and stock material are enclosed in a steel heat shield to minimize heat loss from the edges.

be raised. This temperature limit in turn was seen to limit the strength of the fibers. It is thought that surface cracks in the stock material were not easily removed by pulling at lower temperatures. A further stage of laser polishing was introduced in order to meet the strength requirements for Advanced LIGO.

By varying the speed while pulling the ribbon, it was possible to produce tapered ribbons in a similar manner to the tapered cylindrical fibers.

### III. FIBER PERFORMANCE

The requirements for fiber performance in the Advanced LIGO monolithic suspensions are set out in the design requirements document for cavity optics<sup>49</sup> and the monolithic stage conceptual design document.<sup>50</sup>

The thermal noise requirement for Advanced LIGO suspension fibers is that longitudinal displacement noise must be  $1 \times 10^{-19} \text{ m}/\sqrt{\text{Hz}}$  or less at 10 Hz. Assuming cancellation of the thermoelastic losses, this requirement can be expressed as a limit on the surface loss times the thickness of lossy layer,  $h\phi_{\text{surface}} = 1.9 \times 10^{-11}$ . This is a convenient parameter to choose since it is independent of fiber diameter. A recent publication<sup>51</sup> presenting measurements of the mechanical dissipation in cylindrical fibers produced using this machine shows an average value of  $h\phi_{\text{surface}} = 5 \times 10^{-12} \text{ m}$ . This value is comparable to values for gas pulled fibers<sup>29</sup> of approximately  $h\phi_{\text{surface}} = 5.9 \times 10^{-12} \text{ m}$  and meets the requirement for Advanced LIGO.

Fibers with dimensions suitable for Advanced LIGO were pulled using the machine based at MIT and were destructively strength tested. The fibers were produced using a polishing technique that will be described in a future publication, and had their diameters measured along their length to calculate the stress. The average breaking stress of the fibers was 4.4 GPa. Even the weakest fiber measured would provide a safety margin of three times the working load for either the Virgo or LIGO upgrades.

The requirement for vertical stiffness of 2.8% sets a tolerance on fiber dimensions. In practice this is most easily checked by measurement of the vertical bounce mode of the fiber when loaded. Measurement of the bounce mode of sets of fibers, each loaded with a 1 kg mass, gave a spread of bounce frequencies at the 0.8% level for fibers produced in the same batch, well within the requirements for Advanced LIGO. Assuming that the weight of the test mass is evenly distributed on all four fibers, the length of the fibers needs to be within  $\pm 0.6 \text{ mm}$  of each other to keep the violin modes grouped to within 1 Hz. With fiber lengths varying at the level of 0.3 mm, this requirement should easily be met.

The final requirement is on the position of the fiber flexure point. The tolerance required here is approximately  $\pm 0.1 \text{ mm}$  in horizontal and 1 mm in vertical. The horizontal requirement comes from the static pitch which can be adjusted over a range of 20 Mrad, with the test mass having a pitch compliance of 0.154 rad/N m calculated using a model of the quad suspension.<sup>37</sup> Since this adjustment range must also take into account the tolerance of the ear bonding, we have assumed that the welding tolerance is approximately 6 Mrad

of this adjustment range, corresponding to 0.1 mm in flexure position. The 1 mm tolerance on the vertical position of the flexure point comes from a requirement that the frequency of the first pitch mode of the suspension be above the first longitudinal mode. These tolerances are met by using jigs to hold and move the fibers precisely during welding.

#### IV. WELDING SYSTEMS

To reduce friction in the joints of the mirror suspensions, fused silica fibers are typically welded to fused silica attachment blocks that are hydroxide-catalysis bonded to the sides of the optic.<sup>17–19</sup> The suspensions for GEO600 were welded by hand using a hydrogen–oxygen torch. Again there are advantages to moving to using a laser which offers a more reproducible process.

Two methods of CO<sub>2</sub> laser welding were developed. The first was developed to weld smaller parts that could be placed close to the machine, preferably on the optical bench. The cylindrical fiber pulling machine has a modular design that allows it to be switched to become a welding system by replacement of one section of the machine.

The second scheme was developed to give localized beam delivery when welding larger suspensions that are not on the optical bench. This allows the beam to be delivered to specific weld locations on the Advanced LIGO suspension structure with the beam being enclosed when it is not on the bench.

Both systems use a 130 W CO<sub>2</sub> laser which sets a practical limit to the size of piece that can be welded. It was found that welds could easily penetrate to a depth of around 3 mm using this laser.

##### A. Welding to structures on the optical bench

The design of the fiber pulling machine incorporates the ability for it to be used as a robotic welding system. The system was designed to perform welds to structures located close to or on the optics bench. It is capable of delivering the beam over an area of approximately 1 m<sup>2</sup> in order to reach all the weld locations, but also gives fine control at the submillimeter level to perform fine welds.

The upper conical mirror of the fiber pulling machine, as shown in Fig. 4, is replaced by a double galvanometer head giving a fine x–y delivery of the beam using a joystick control. The galvanometers are mounted on the horizontal ballscrew which in turn is mounted on the vertical ballscrew unit. These give the galvanometer head a wide range motion of 1 m horizontally and 1.2 m vertically, and again are joystick controlled. The laser is then rerouted using a flipper mirror to travel vertically up the side of the machine and along the horizontal arm to the galvanometers, from where it can be directed to the weld location. Each of the three fiber pulling machines is equipped with this system. For practical reasons the horizontal ballscrew unit can be removed from the machine when not in use, for example, when using the alternative welding system to build suspensions.



FIG. 9. (Color) The welding system consists of a CO<sub>2</sub> laser delivered through an articulated arm, ZnSe output telescope, and a pair of mirror galvanometers.

##### B. Welding to remote structures

When welding to structures that cannot easily be located on the optical bench, it is safer and easier to use an enclosed beam that can be delivered to different locations. A remote welding system was devised based on a commercially available Zeiss articulated arm, as shown in Fig. 9. This arm contains gold coated mirrors mounted at 45° in each joint. At each of these joints, the arm is constrained to rotate only about the optical axis along which the laser beam is traveling allowing the beam to stay centered on each mirror along the arm's length once it has been aligned.

At the end of the arm, ZnSe lenses are used to focus the beam. The lenses form a compact telescope 10 cm in length. The separation of the lenses can be altered, allowing the power density and diameter to be varied at the welding point. A calibration chart was produced for the telescope, giving the beam diameter at the weld location as a function of lens separation.

From the telescope, the beam is reflected from two mirror galvanometers, as shown in Fig. 10, that are mounted at right angles to each other on the end of the arm. The mirror galvanometers are servo controlled, with the positional

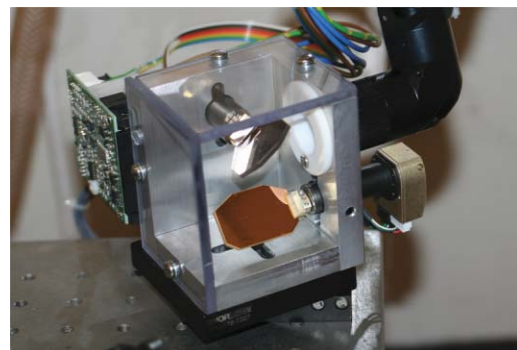


FIG. 10. (Color) A pair of computer controlled mirror galvanometers are used to move the laser over the weld region.



information coming from a custom LABVIEW script. The program is preset to limit the movement of the galvanometers to keep the beam within the area of the weld so as to increase safety. The beam can then be moved over the weld using the computer cursor keys. The beam can also be dithered over the weld area by scanning the beam using a continuous wave input. Using the articulated arm, the galvanometers can be moved to predetermined locations on the suspension structure close to the ends of the fiber before fixing the position of the end of the arm, and performing the weld.

## V. CONCLUSIONS

A CO<sub>2</sub> laser-based fused silica fiber pulling machine was developed that is capable of meeting requirements for strength, thermal noise performance, and dimensional tolerance for the next generation of gravitational wave detector mirror suspensions. The ability to produce circular and rectangular cross-section fibers was developed, as well as tapering along the length of the fiber. Two laser welding methods were investigated, allowing for smaller parts to be welded on the optical bench, and large suspensions such as those planned for Advanced LIGO, to be welded by delivering the beam to the weld locations using an articulated arm. The MIT-based machine has been used to build the monolithic suspension for the LASTI noise prototype and will soon be relocated to the Hanford LIGO site where it will be used to produce suspension fibers for Advanced LIGO. The separate welding system for use on remote structures will be used for welding the suspensions close to the vacuum tanks at the Hanford and Livingston LIGO sites. The machine at the Virgo site has been used to build a prototype suspension for the Virgo upgrade, and is now being used to produce the new suspensions for the interferometer at the site.

## ACKNOWLEDGMENTS

The authors would like to thank Colin Craig and Stephen Craig for their work toward the construction of the laser fiber pulling machine. We would like to thank our colleagues in the GEO600 project, the Scottish Universities Physics Alliance (SUPA), and the LIGO Scientific Collaboration for their interest in this work. We also wish to thank the ILIAS Strega project and Leverhulme Trust for support. We are grateful for the financial support provided by the STFC and the University of Glasgow in the UK and the NSF in the USA. The LIGO Observatories were constructed by the California Institute of Technology and Massachusetts Institute of Technology with funding from the NSF under cooperative agreement PHY-9210038. The LIGO Laboratory operates under cooperative agreement PHY-0107417.

<sup>1</sup>H. B. Callen and T. A. Welton, *Phys. Rev.* **83**, 34 (1951).

<sup>2</sup>H. B. Callen and R. F. Greene, *Phys. Rev.* **86**, 702 (1952).

<sup>3</sup>P. R. Saulson, *Phys. Rev. D* **42**, 2437 (1990).

<sup>4</sup>Y. Levin, *Phys. Rev. D* **57**, 659 (1998).

<sup>5</sup>S. Rowan, J. Hough, and D. Crooks, *Phys. Lett. A* **347**, 25 (2005).

<sup>6</sup>V. Braginsky, V. Mitrofanov, and O. Okhrimenko, *Phys. Lett. A* **175**, 82 (1993).

<sup>7</sup>V. B. Braginsky, V. P. Mitrofanov, and K. V. Tokmakov, *Phys. Lett. A* **186**, 18 (1994).

<sup>8</sup>S. Rowan, S. M. Twyford, R. Hutchins, J. Kovalik, J. E. Logan, A. C. McLaren, N. A. Robertson, and J. Hough, *Phys. Lett. A* **233**, 303 (1997).

<sup>9</sup>A. Ageev, B. C. Palmer, A. D. Felice, S. D. Penn, and P. R. Saulson, *Class. Quantum Grav.* **21**, 3887 (2004).

<sup>10</sup>K. Numata, K. Yamamoto, H. Ishimoto, S. Otsuka, K. Kawabe, M. Ando, and K. Tsubono, *Phys. Lett. A* **327**, 263 (2004).

<sup>11</sup>S. D. Penn, A. Ageev, D. Busby, G. M. Harry, A. M. Gretarsson, K. Numata, and P. Willems, *Phys. Lett. A* **352**, 3 (2006).

<sup>12</sup>V. B. Braginsky, V. P. Mitrofanov, and V. I. Panov, in *Systems with Small Dissipation*, edited by K. S. Thorne (University of Chicago Press, Chicago, 1986).

<sup>13</sup>Y. L. Huang and P. R. Saulson, *Rev. Sci. Instrum.* **69**, 544 (1998).

<sup>14</sup>G. Cagnoli, L. Gammaitoni, J. Kovalik, F. Marchesoni, and M. Punturo, *Phys. Lett. A* **255**, 230 (1999).

<sup>15</sup>G. Cagnoli, L. Gammaitoni, J. Kovalik, F. Marchesoni, and M. Punturo, *Phys. Lett. A* **213**, 245 (1996).

<sup>16</sup>B. Willke, P. Aufmuth, C. Aulbert, S. Babak, R. Balasubramanian, B. W. Barr, S. Berukoff, S. Bose, G. Cagnoli, M. M. Casey, D. Churches, D. Clubley, C. N. Colacino, D. R. M. Crooks, C. Cutler, K. Danzmann, R. Davies, R. Dupuis, E. Elliffe, C. Fallnich, A. Freise, S. Gossler, A. Grant, H. Grote, G. Heinzel, A. Heptonstall, M. Heurs, M. Hewitson, J. Hough, O. Jennrich, K. Kawabe, K. Kotter, V. Leonhardt, H. Luck, M. Malec, P. W. McNamara, S. A. McIntosh, K. Mossavi, S. Mohanty, S. Mukherjee, S. Nagano, G. P. Newton, B. J. Owen, D. Palmer, M. A. Papa, M. V. Plissi, V. Quetschke, D. I. Robertson, N. A. Robertson, S. Rowan, A. Rudiger, B. S. Sathyaprakash, R. Schilling, B. F. Schutz, R. Senior, A. M. Sintes, K. D. Skeldon, P. Sneddon, F. Stief, K. A. Strain, I. Taylor, C. I. Torrie, A. Vecchio, H. Ward, U. Weiland, H. Welling, P. Williams, W. Winkler, G. Woan, and I. Zawischa, *Class. Quantum Grav.* **19**, 1377 (2002).

<sup>17</sup>D. Gwo, U.S. patent 6,548,176 B1 (2003).

<sup>18</sup>S. Rowan, S. M. Twyford, J. Hough, D. H. Gwo, and R. Route, *Phys. Lett. A* **246**, 471 (1998).

<sup>19</sup>P. H. Sneddon, S. Bull, G. Cagnoli, D. R. M. Crooks, E. J. Elliffe, J. E. Faller, M. M. Fejer, J. Hough, and S. Rowan, *Class. Quantum Grav.* **20**, 5025 (2003).

<sup>20</sup>S. Goßler, G. Cagnoli, D. R. M. Crooks, H. Lück, S. Rowan, J. R. Smith, K. A. Strain, J. Hough, and K. Danzmann, *Class. Quantum Grav.* **21**, S923 (2004).

<sup>21</sup>B. Sorazu, K. A. Strain, I. S. Heng, and R. Kumar, *Class. Quantum Grav.* **27**, 155017 (2010).

<sup>22</sup>N. A. Robertson, G. Cagnoli, D. R. M. Crooks, E. Elliffe, J. E. Faller, P. Fritschel, S. Goßler, A. Grant, A. Heptonstall, J. Hough, H. Lück, R. Mittleman, M. Perreux-Lloyd, M. V. Plissi, S. Rowan, D. H. Shoemaker, P. H. Sneddon, K. A. Strain, C. I. Torrie, H. Ward, and P. Willems, *Class. Quantum Grav.* **19**, 4043 (2002).

<sup>23</sup>P. Amico, L. Bosi, L. Carbone, L. Gammaitoni, M. Punturo, F. Travasso, and H. Vocca, *Class. Quantum Grav.* **19**, 1669 (2002).

<sup>24</sup>SOLIDWORKS 3D CAD Software, Dassault Systemes SolidWorks Corp., Concord, Massachusetts, USA.

<sup>25</sup>A. S. Nowick and B. S. Berry, *Anelastic Relaxation in Crystalline Solids* (Academic, New York, 1972).

<sup>26</sup>C. Zener, *Phys. Rev.* **53**, 90 (1938).

<sup>27</sup>G. Cagnoli and P. A. Willems, *Phys. Rev. B* **65**, 174111 (2002).

<sup>28</sup>J. Wiedersich, S. V. Adichtchev, and E. Rössler, *Phys. Rev. Lett.* **84**, 2718 (2000).

<sup>29</sup>A. M. Gretarsson and G. M. Harry, *Rev. Sci. Instrum.* **70**, 4081 (1999).

<sup>30</sup>P. Willems, V. Sannibale, J. Weel, and V. Mitrofanov, *Phys. Lett. A* **297**, 37 (2002).

<sup>31</sup>A. Heptonstall, G. Cagnoli, J. Hough, and S. Rowan, *Phys. Lett. A* **354**, 353 (2006).

<sup>32</sup>N. A. Robertson, M. Barton, and J. Greenhalgh, LIGO Document No. T040143, 2004, available at <https://dcc.ligo.org/>.

<sup>33</sup>G. Cagnoli and C. A. Cantley, LIGO Document No. T050212, 2005, available at <https://dcc.ligo.org/>.

<sup>34</sup>G. Cagnoli, J. Hough, D. DeBra, M. M. Fejer, E. Gustafson, S. Rowan, and V. Mitrofanov, *Phys. Lett. A* **272**, 39 (2000).

<sup>35</sup>P. Willems, *Phys. Lett. A* **300**, 162 (2002).

<sup>36</sup>M. Barton, A. Heptonstall, C. Craig, A. Cumming, L. Cunningham, G. Hammond, K. Haughian, J. Hough, R. Jones, R. Kumar, N. Robertson, S. Rowan, K. Strain, K. Tokmakov, C. Torrie, and M. V. Veggel, LIGO Document No. T080091, 2008, available at <https://dcc.ligo.org/>.



- <sup>37</sup>M. Barton, LIGO Document No. T1000263, 2010, available at <https://dcc.ligo.org/>.
- <sup>38</sup>J. D. Strong, *Procedures in Experimental Physics* (Prentice-Hall, Englewood Cliffs, NJ, 1938).
- <sup>39</sup>T. T. O'Donnell, *Drawing and Working Quartz Fibers* (National Academy of Sciences—National Research Council, Washington, 1958).
- <sup>40</sup>S. Rowan, R. Hutchins, A. McLaren, N. A. Robertson, S. M. Twyford, and J. Hough, *Phys. Lett. A* **227**, 153 (1997).
- <sup>41</sup>A. Cavalleri, G. Ciani, R. Dolesi, A. Heptonstall, M. Hueller, D. Nicolodi, S. Rowan, D. Tombolato, S. Vitale, P. J. Wass, and W. J. Weber, *Class. Quantum Grav.* **26**, 094017 (2009).
- <sup>42</sup>A. Cavalleri, G. Ciani, R. Dolesi, A. Heptonstall, M. Hueller, D. Nicolodi, S. Rowan, D. Tombolato, S. Vitale, P. J. Wass, and W. J. Weber, *Phys. Rev. Lett.* **103**, 140601 (2009).
- <sup>43</sup>V. P. Mitrofanov, O. I. Ponomareva, and A. A. Khorev, *Zh. Tekh. Fiz.* **55**, 765 (1985).
- <sup>44</sup>V. K. Sysoev, B. P. Papchenko, and S. Y. Rusanov, *Glass Ceram.* **61**, 106 (2004).
- <sup>45</sup>G. Harry, T. Corbitt, M. Freytsis, D. Ottaway, N. Mavalvala, and S. Penn, *Rev. Sci. Instrum.* **77**, 023906 (2006).
- <sup>46</sup>C. Kurkjian, J. Krause, and M. Matthewson, *J. Lightwave Technol.* **7**, 1360 (1989).
- <sup>47</sup>P. Willems and M. Thattai, *Phys. Lett. A* **253**, 16 (1999).
- <sup>48</sup>A. Cumming, A. Heptonstall, R. Kumar, W. Cunningham, C. Torrie, M. Barton, K. A. Strain, J. Hough, and S. Rowan, *Class. Quantum Grav.* **26**, 215012 (2009).
- <sup>49</sup>M. Barton, N. Robertson, P. Fritschel, D. Shoemaker, and P. Willems, LIGO Document No. T010007, 2008, available at <https://dcc.ligo.org/>.
- <sup>50</sup>C. A. Cantley, H. Armandula, M. Barton, G. Cagnoli, A. Cumming, D. Crooks, E. Elliffe, R. J.S. Greenhalgh, T. Hayler, A. Heptonstall, J. Hough, R. Jones, J. O'Dell, I. Martin, M. Perreux-Lloyd, N. A. Robertson, J. Romie, S. Rowan, K. A. Strain, C. Torrie, and I. Wilmot, LIGO Document No. T050215, 2005, available at <https://dcc.ligo.org/>.
- <sup>51</sup>A. Heptonstall, M. Barton, C. Cantley, A. Cumming, G. Cagnoli, J. Hough, R. Jones, R. Kumar, I. Martin, S. Rowan, C. Torrie, and S. Zech, *Class. Quantum Grav.* **27**, 035013 (2010).